Draft version September 2, 2022
Typeset using LaTeX **twocolumn** style in AASTeX63

Fixed-scale analyses on giant molecular clouds in observed and simulated galaxy mergers

Hao He,[1] Christine Wilson,[1] Connor Bottrell,[2] and Jorge Moreno[3]

[1] *McMaster University*
1280 Main St W, Hamilton, ON L8S 4L8, CAN
[2] *Kavli Institute for the Physics and Mathematics of the Universe (WPI), UTIAS, University of Tokyo*
Kashiwa, Chiba 277-8583, Japan
[3] *Department of Physics and Astronomy, Pomona College,*
Claremont, CA 91711, USA

(Received September 2, 2022; Revised xxx; Accepted xxx)

Submitted to ApJ Letter

ABSTRACT

We employ the Feedback In Realistic Environments (FIRE-2) physics model to study how the properties of giant molecular clouds (GMCs) evolve during galaxy mergers. Due to the rarity of mergers in the local Universe, samples of nearby merging galaxies suitable for studies of individual GMCs are limited. Idealized simulations provide us with a new window to study GMC evolution during a merger, and assist in interpreting observations. We conduct a pixel-by-pixel analysis of the simulated molecular gas properties in both undisturbed control galaxies and galaxy mergers. The simulated GMCs follow a similar trend in a plot of velocity dispersion versus gas surface density as observed in normal spiral galaxies in the Physics at High Angular resolution in Nearby GalaxieS (PHANGS) survey. However, the gas surface density of the simulated galaxies sits at the lower surface density end compared to PHANGS galaxies, with a maximum surface density of 100 $M_\odot$ pc^{-2}. In fact, the simulated data lie closer to the regime of dwarf galaxies or green valley galaxies such as M31. We suspect the low gas surface densities are driven by the low gas mass fraction due to the choice of initial conditions in the simulations. For the simulated mergers, we find the gas surface density is still low compared to two observed mergers. On the other hand, the gas in simulated mergers has a high velocity dispersion that is comparable to the observed mergers. The virial parameters of GMCs in the simulated mergers are much higher than those of normal spiral galaxies both in observations and simulations. These high virial parameters are consistent with the expectation that feedback from starburst episodes will unbind and disperse the surrounding GMCs.

Keywords: ISM: clouds, ISM: kinematics and dynamics, ISM: structure, galaxies: interactions, galaxies: starburst, galaxies: star formation

1. INTRODUCTION

Giant molecular clouds (GMCs) are the birth places of stars. Hence, to understand the links between molecular gas and star formation rate (SFR) in galaxies, it is essential to study the physical properties of molecular clouds in a broad range of environments. Some theoretical frameworks suggest that the large scatter in depletion times ($t_{\rm dep} = M_{\rm H_2}/{\rm SFR}$) observed on GMC scales can be explained by the diversity in the GMC population (Feldmann & Gnedin 2011; Kruijssen et al. 2014; Grudić et al. 2018; Kruijssen et al. 2018). However, some observations (Lee et al. 2016) still find discrepancies between the observed and simulated scatter in $t_{\rm dep}$. The modeling of GMCs is further complicated by challenges in capturing the structure of the coldes and densest gas, which are heavily affected by various numerical choices, such as resolution (e.g. Bournaud et al. 2008; Teyssier

Corresponding author: Hao He
heh15@mcmaster.ca

et al. 2010) (references in Benicasa+2014, pg13) and the treatment of feedback (Fall et al. 2010; Murray et al. 2010; Dale et al. 2014; Myers et al. 2014; Raskutti et al. 2016; Kim et al. 2017; Grudić et al. 2018). Most GMC simulations focus on the evolution of individual GMCs (e.g. Howard et al. 2018; Li et al. 2019; Decataldo et al. 2020) and ignore their environment. Only a handful of galaxy simulations have the ability to model GMC populations inside Milky-Way-like galaxies (Jeffreson & Kruijssen 2018; Benincasa et al. 2020) and mergers (Renaud et al. 2019a; Li et al. 2022).

High-resolution CO observations have successfully characterized GMCs in the Milky Way (e.g. Rice et al. 2016; Rico-Villas et al. 2020; Miville-Deschênes et al. 2017; Colombo et al. 2019; Lada & Dame 2020) and nearby galaxies (e.g. Donovan Meyer et al. 2013; Hughes et al. 2013; Colombo et al. 2014; Leroy et al. 2016; Schruba et al. 2019). In particular, the recently completed PHANGS-ALMA survey (Leroy et al. 2021)have expanded these observations across a complete sample of nearby spiral galaxies, providing direct measurements of molecular gas surface density $\Sigma_{\rm mol}$, velocity dispersion σ_v and radius R, which are key quantities for determining the physical state of GMCs (Larson 1981). Observations show that the correlation between σ_v^2/R and $\Sigma_{\rm mol}$ is nearly linear (e.g., Heyer & Dame 2015; Sun et al. 2018, 2020), which is consistent with the theoretical prediction that most clouds are in a state of equilibrium between kinetic and gravitational potential energy (Larson's second law; Larson 1981). This universal correlation provides us with a starting point to study how other galactic environmental factors (e.g., external pressure, stellar potential) influence the dynamical state of GMCs.

In both observations and theory, GMCs in galaxy mergers are rarely studied. On the observational side, the scarcity of nearby mergers means that we only have handful of systems observed with GMC resolution (Brunetti et al. 2020; Brunetti 2022, Ph.D. thesis; Brunetti et al., in prep.). These studies show that GMCs in mergers have significantly higher gas surface densities and are less gravitationally bound compared to GMCs in normal spirals. However, it is difficult to draw statistically robust conclusions on how GMC properties evolve across various merging stages based on these limited observational samples. On the simulation front, few studies exists due to limitations in sub-grid modelling (e.g., Teyssier et al. 2010; Renaud et al. 2014; Fensch et al. 2017). Using a comprehensive library of idealized galaxy merger simulations based on the FIRE-2 physics model, Moreno et al. (2019) show that SFR enhancement is accompanied by an increase in the cold dense gas reservoir. This suite thus provides us with the ideal tool to properly examine GMC evolution along the entire merging sequence.

This paper explores correlations of basic GMC properties using the FIRE-2 merger suite from Moreno et al. (2019) and performs comparisons with observations. In Section 2, we describe this simulation suite and the observational data used for comparison. Section 3 compares the σ_v $-\Sigma_{\rm mol}$ relation between control simulated galaxies and normal spirals in PHANGS-ALMA sample. Section 4 examines the σ_v $-\Sigma_{\rm mol}$ relation for mergers in both observations and simulations. In Section 5, we discuss and interpret various aspects of the comparison between observation and simulation results.

2. DATA PROCESSING

2.1. *Simulated data*

2.1.1. *The FIRE-2 Model*

We use the FIRE-2 model (Hopkins et al. 2018), which employs the hydrodynamic code GIZMO (Hopkins 2015, 2017). We refer the reader to Hopkins (2015) and Hopkins et al. (2018) for details. The model includes treatment of radiative heating and cooling from free-free, photo-ionization/recombination, Compton, photoelectric, dust-collisional, cosmic ray, molecular, metal line and fine-structure processes. Star formation occurs in gas that is self-gravitating (at the resolution scale), self shielded and denser than 1000 cm^{-3} using a multi free-fall time approach (see Appendix C of Hopkins et al. 2018). Stellar feedback mechanisms include (i) mass, metal, energy and momentum flux from supernovae type Ia & II; (ii) continuous stellar mass-loss through OB/AGB winds; (iii) photoionization and photoelectric heating; and (iv) radiation pressure. Each stellar particle is treated as a single stellar population. Mass, age, metallicity, luminosity, energy, mass-loss rate, and stellar feedback event rate for each stellar particle are calculated using the STARBURST99 stellar population synthesis model (Leitherer et al. 1999). The model does not account for feedback generated via accretion of gas onto a supermassive black hole (SMBH). SMBH feedback is omitted because uncertain physical processes behind the coupling between an AGN and the circumnuclear interstellar medium (ISM) are still under exploration (Torrey et al. 2017; Wellons et al. 2022).

2.1.2. *Our merger suite*

Moreno et al. (2019) present a suite of idealized galaxy merger simulations (see also Bottrell et al. 2019; Moreno et al. 2021; McElroy et al. 2022) covering a range of orbital parameters and mass ratios between 4 disc galaxies (G1, G2, G3 and G4, in order of increasing total stellar

mass of 2.1×10^9 $M_\odot$, 1.24×10^{10} $M_\odot$, 2.97×10^{10} $M_\odot$ and 5.5×10^{10} $M_\odot$), along with separate runs for each disk galaxy in isolation (the control runs). Their orbit settings contain 3 orbital spin directions, 3 impact parameters and 3 impact velocities (see Fig. 3 in Moreno et al. 2019). For these simulations, the highest gas density and spatial resolution are 5.8×10^5 cm^{-3} and 1.1 pc, respectively. The gravitational softening lengths are 10 pc for the dark matter and stellar components and 1 pc for the gaseous component. These scales are smaller than the typical scale of observed GMCs (40 – 100 pc, references needed). The time resolution of a typical snapshot is 5 Myr. Please see Moreno et al. (2019) for details.

For our analysis, we focus on one of the G2&G3 merger suites, which is a major merger with a mass ratio of 1:2.5 and hence is similar to major mergers such as Antennae and NGC 3256 for which we have GMC observational data. In addition, G2 and G3 have stellar masses within the range of the PHANGS sample (10^{10} – 10^{11} $M_\odot$; Leroy et al. 2021). We choose the 'e' (Robertson et al. 2006, roughly prograde) orbit, which is expected to maximally enhance the star formation rate.

2.1.3. *Molecular gas*

We follow the scheme in Moreno et al. (2019) to separate the ISM into 4 components based on its temperature and density: hot, warm, cool and cold-dense gas, which roughly correspond to the hot, ionized, atomic and molecular gas in observations. The components that are most important for this work are the cool and the cold-dense gas, which have temperatures below 8000 K and density above 0.1 cm^{-3}. This choice captures HI and H_2 gas reasonably well (Orr et al. 2018). Orr et al. (2018) also demonstrate that using this threshold to separate H_2 and HI yields reasonable agreement with the observed Kennicutt-Schmidt law (Kennicutt 1998; Kennicutt & Evans 2012). In the following, we refer to total gas as the sum of the gas in the cool and cold-dense phases (simulations) or in the atomic and molecular phases (observations).

We adopt the same definition of molecular gas as in Moreno et al. (2019) (temperature below 300 K and density above 10 cm^{-3}). Guszejnov et al. (2017) demonstrate that the model successfully reproduces the GMC mass function in the Milky Way (Rice et al. 2016) and the line-width size relation (e.g., the Larson scaling relationship, Larson 1981) in our Galaxy (Heyer et al. 2009; Heyer & Dame 2015) and in nearby galaxies (Bolatto et al. 2008 Fukui et al. 2008; Muraoka et al. 2009; Roman-Duval et al. 2010; Colombo et al. 2014; Tosaki et al. 2017).

We note that these simulations start with a homogeneous ISM with a temperature of 10^4 K and solar metallicity. The multi-phase ISM then emerges quicly as a result of feedback from the star formation. The initial gas mass for the simulation is set to match the median HI mass from the xCOLDGASS survey (Catinella et al. 2018). As shown in Moreno et al. (2019), about 2/3 of the gas transforms to the warm and hot phases when the simulation run reaches steady-state. As a result, the total gas fraction (atomic plus molecular) relative to the stellar mass will be about 3 times lower than that of representative spiral galaxies in our local universe, as shown in Section 3.2 below. This low gas fraction may be the cause of the low values for $\Sigma_{\rm mol}$ we measure for the simulated galaxies (see Section 3, 4)

2.1.4. *Data cubes*

We first convert the FIRE-2 molecular gas data into position-position-velocity (p-p-v) data cubes to match the format of the CO data from radio observations (McMullin et al. 2007). We adopt the cube construction method that was created for Bottrell et al. (2022) and Bottrell & Hani (2022) using TNG and then adapted to the FIRE-2 merger suite for (McElroy et al. 2022). Kinematic cubes are produced along four lines-of-sight (labeled as 'v0', 'v1', 'v2', 'v3'), defined by the vertices of a tetrahedron centred at the primary galaxy (G3 in this work). For the isolated galaxy simulations, we generate position-position-velocity (p-p-v) data cubes at different inclination angles (10 – 80 degrees). We adopt a pixel size of 100 pc and velocity resolution of 2 km s^{-1}.

Then we create zeroth-moment maps of the gas surface density $\Sigma_{\rm mol}$ and second-moment maps of the velocity dispersion σ_v. We do not set any thresholds on these moment maps since we argue that every gas particle in the simulated cube should be treated as a real signal, rather than observational noise. However, in later analyses when we display σ_v versus $\Sigma_{\rm mol}$ for the simulated data, we select pixels with $\Sigma_{\rm mol}$ greater than 1 $M_\odot$ pc^{-2}, which approximates the lower limit of the molecular gas detection threshold in the observational data (Sun et al. 2018). We also exclude pixels detected in fewer than two velocity channels in the simulated cube to exclude inaccurate measurements of σ_v.

To characterize clouds, we use a fixed-scale analysis (Leroy et al. 2016), which treats each pixel as an individual GMC, rather than identifying each individual cloud from the data cube. This approach has been widely applied to GMC analyses for PHANGS galaxies (Sun et al. 2018, 2020). Compared to the traditional cube-based approach, this new method requires minimal assumptions and can be easily applied to many datasets in

a uniform way, while still giving us the essential GMC properties (e.g., molecular gas surface density $\Sigma_{\rm mol}$, gas velocity dispersion σ_v). Sun et al. (2022) compared this new approach with the traditional approach and find general agreement on cloud properties for PHANGS galaxies. Furthermore, Brunetti & Wilson (2022) have made a similar comparison between the two methods for NGC 3256, a luminous infrared galaxy (LIRG), and also find good agreement between the two methods. These studies show that a fixed-scale analysis should be valid for our measurements from the simulation data. In this work, we adopt this approach to match the method in Brunetti et al. (2020) and Brunetti (2022, Ph.D. thesis).

2.2. *Observational Data*

2.2.1. *Spiral galaxies: PHANGS data*

We use several sets of observations for comparison with our simulations. For isolated galaxies, we mainly use the PHANGS data from Sun et al. (2020) with resolution of 90 pc. Sun et al. (2020) apply the fixed-scale method for statistical analyses of GMC properties for 70 galaxies in the PHANGS sample. We also include GMC data for M31 from Sun et al. (2018) at resolution of 120 pc. M31 is identified as a green-valley galaxy, similar to our own Milky Way, and hence has a lower total gas fraction than normal spiral galaxies (Mutch et al. 2011). Both M31 and the Milky Way seem to be in a transition from blue spiral galaxies to quenched galaxies via depletion of their cold gas. M31 has stellar mass of 10^{11} $M_\odot$ (Sick et al. 2015), H_2 mass of 3.6×10^8 $M_\odot$ and H I mass of 4.8×10^9 $M_\odot$ (Nieten et al. 2006).

2.2.2. *Galxy mergers: the Antennae and NGC 3256*

We use the GMC data for NGC 3256 (Brunetti et al. 2020) and the Antennae (Brunetti, 2022, PhD thesis, and Brunetti, N et al. in prep) at resolutions of 90 and 80 pc, respectively. The GMC measurements use the same fixed-scale approach as in Sun et al. (2018, 2020). Both NGC 3256 and the Antennae are identified as late-stage major mergers that have been through their second perigalactic passage (Privon et al. 2013). NGC 3256 has stellar mass of 1.1×10^{11} $M_\odot$ and SFR of 50 $M_\odot yr^{-1}$ (Sakamoto et al. 2014). In contrast, the Antennae has a stellar mass of 4.5×10^{10} $M_\odot$ and SFR of 8.5 $M_\odot yr^{-1}$ (Seillé et al. 2022). NGC 3256 currently has a more intense starburst, perhaps because it is at different evolutionary stage in the merging process.

2.2.3. *Global gas measurements*

On global scales, we compare the molecular gas mass and total gas mass (including HI) of the FIRE-2 galaxies with observed values for normal spiral galaxies. We compare to both the PHANGS galaxies (Leroy et al. 2021) as well as to the global gas properties from the xCOLDGASS survey, to confirm that the PHANGS galaxies are representative of star forming main sequence galaxies in our local universe. For xCOLDGASS, the molecular gas mass is extracted from Saintonge et al. (2017) and the total gas mass is from Catinella et al. (2018).

3. CONTROL (ISOLATED) GALAXIES

3.1. *GMC linewidth and surface density*

To test if the simulation successfully reproduces observed GMCs, Figure 1 shows the well-known correlation between σ_v and $\Sigma_{\rm mol}$ for isolated simulated galaxies and PHANGS-ALMA spiral galaxies. The left panel shows σ_v versus $\Sigma_{\rm mol}$ contour for G2 and G3 galaxies at inclination angle of 30 degrees compared with that of observed galaxies, while the right contour shows the contour for G3 galaxies with different inclination angles. The two simulated galaxies, G2 and G3, exhibit similar properties (black and dark red solid contours) and generally lie on the trend followed by the PHANGS galaxies when viewed at an inclination angle of 30 degrees. We also plot the red dashed line indicating GMCs with constant virial parameter $\alpha_{\rm vir}$ of 3.1. We can see both our simulated galaxies and observed PHANGS galaxies follows the trend of the constant $\alpha_{\rm vir}$, which gives the relation of $\sigma_v^2 \propto \Sigma_{\rm mol}$. On this aspect, the simulation reproduce GMCs similar to the observation. However, we can see that the two galaxies lie at the low surface-density end of the PHANGS distribution and thus their gas properties are more similar to those of M31 than to a typical PHANGS galaxy.

One important factor that might influence $\Sigma_{\rm mol}$ measured from the simulations is the inclination angle at which the galaxy is viewed. Since the inclination angles for PHANGS galaxies are 30 – 60 degrees, the right panel of Fig. 1 shows the data for the G3 galaxy viewed with inclination angles of 30, 60 and 80 degrees. We see little increase in $\Sigma_{\rm mol}$ even for an inclination of 80 degrees. This is consistent with our expectation that individual clouds are resolved in the simulated data. For resolved spherical clouds, the observed surface density should always be the same despite different viewing angles.

3.2. *Global gas fraction*

In interpreting the lower $\Sigma_{\rm mol}$ values seen in Fig. 1, one possibility is that there may not be as much gas available to form high surface density clouds in the two simulated galaxies compared to the PHANGS galaxies. Fig. 2 compares the global molecular gas masses, $M_{\rm mol}$,

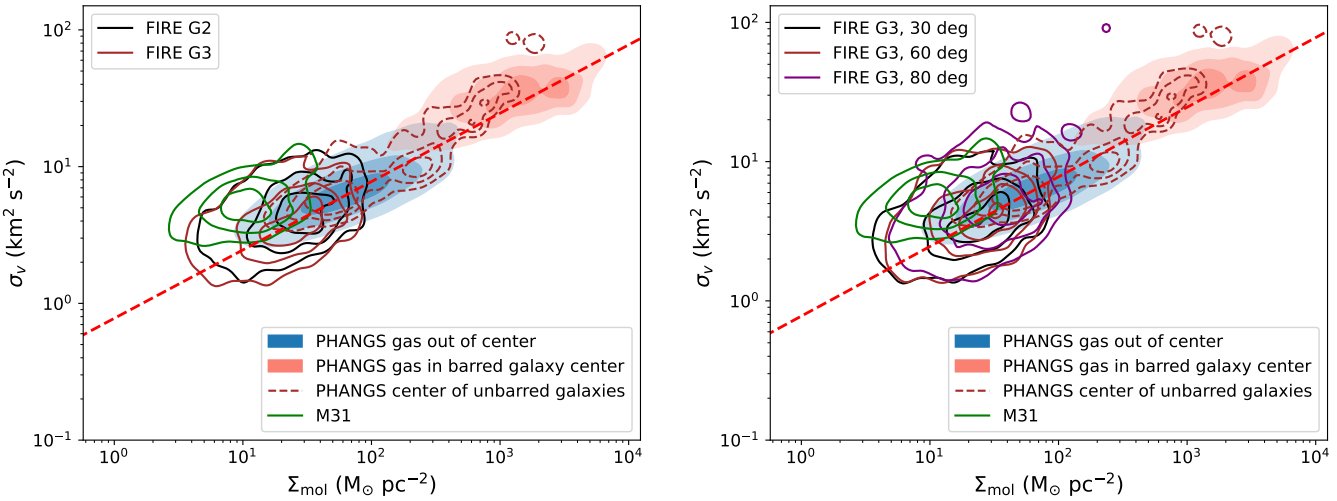

Figure 1. (Left) velocity dispersion versus gas surface density for the G2 (black solid line) and G3 (brown solid line) simulated galaxies with inclination angle of 30 degrees compared to the PHANGS galaxy sample. The contour is mass weighted and set to include 20%, 50% and 80% of the data. The density contours of PHANGS galaxies (Sun et al. 2020) show the distribution of measurements in galaxy disks (blue shaded contours), the centers of barred galaxies (Salmon shaded contours) and the centers of unbarred galaxies (brown dashed contours) with a resolution of 90 pc. The red dashed line marks the position with median values of α_{vir} for PHANGS galaxies of 3.1 (Sun et al. 2020). We also show the data for M31 (green solid contour) at 120 pc resolution from Sun et al. (2018). Σ_{mol} and σ_v for the FIRE-2 spiral galaxies follow a similar trend to the PHANGS galaxies but lie at the lower end of the plot. (Right) Similar to the left panel but with the simulated G3 galaxy viewed at different inclination angles (30, 60 and 80 degrees).

and molecular gas fractions, $f_{mol} = M_{mol} / M_\star$, for the FIRE-2 mergers with those of the PHANGS galaxies from Sun et al. (2020). We also show the median value of M_{mol} and f_{gas} in each $M_\star$ bin for the PHANGS galaxies, as well as the weighted median of $M_\star$ and f_{mol} for galaxies in xCOLDGASS sample (Saintonge et al. 2017). The two median values are quite close to each other for galaxies with $M_\star$ of $10^{9.5}$ – 10^{11} M$_\odot$, although the PHANGS galaxies seem to deviate somewhat from the xCOLDGASS sample in the highest and lowest mass bins. In contrast, the G2 and G3 galaxies both have f_{mol} $\sim$ 3 times lower than typical PHANGS or xCOLDGASS galaxies of the same stellar mass. Therefore, the small global f_{mol} may be the cause for producing the low Σ_{mol} values seen in the simulated galaxies.

The low values of f_{mol} could be produced either by the initial set-up of the simulations or by physical mechanisms in the simulation that lead to inefficient conversion of gas into the cold phase. We can distinguish between these two options by calculating the total gas fraction f_{gas} including both HI and H_2. The lower panel of Fig. 2 shows the median of M_{gas} and f_{gas} for the PHANGS galaxies and xGASS-CO samples (Catinella et al. 2018), against the two simulated galaxies. f_{gas} values for both simulated galaxies are still $\sim$ 3 times lower than those of typical spiral galaxies with similar $M_\star$. Therefore, it seems most likely that the low cold gas fraction, f_{mol}, is produced by a low total (cold+warm+hot) gas mass in the initial set-up of the simulations.

4. MERGING GALAXIES

4.1. *GMC linewidth and surface density*

We performed a similar σ_v versus Σ_{mol} analysis for our suite of galaxy merger simulations. We are particularly interested to see whether the low Σ_{mol} seen in the isolated galaxies results in low gas surface densities in the mergers. We focus on the period when the starburst is most intense to see if Σ_{mol} has significantly increased during that period, since the molecular gas surface density should be proportional to SFR surface density according to the Kennicutt-Schmidt law (Kennicutt & Evans 2012). Fig. 3 shows the variation of the mass weighted median value of Σ_{mol} and σ_v during the second collapse of the simulated mergers. As we can see, both Σ_{mol} and σ_v has significantly increased during the merging event, with maximal increase by a factor of 10. The increase in σ_v and Σ_{mol} is roughly of the same order. However, as we mentioned in Section 3.1, a constant α_{vir} requires $\sigma_v^2 \propto \Sigma_{mol}$. Therefore, we would expect our simulated merger shows higher α_{vir} and lies above the trend shown for PHANGS galaxies in σ_v vs Σ_{mol} plots.

In Fig. 4 and 5 we show some example snapshots of σ_v versus Σ_{mol} for different merger stages during the second passage along with moment 0 maps at each snap-

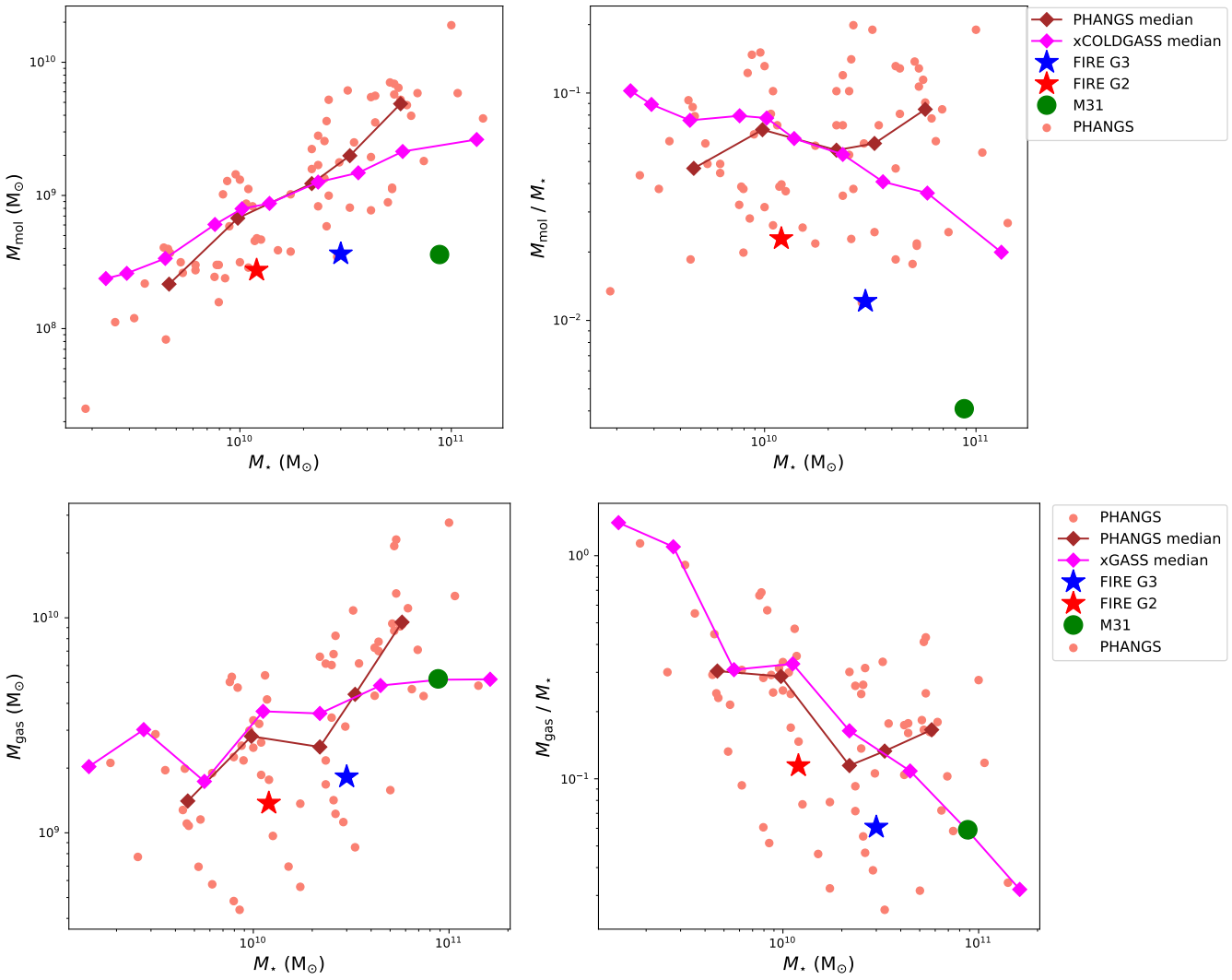

Figure 2. (Upper Left) $M_{\rm mol}$ versus $M_\star$ for PHANGS galaxies (salmon dots; Leroy et al. 2021), M 31 (green filled circle; Nieten et al. 2006) and the G2 (red star) and G3 (blue star) simulated galaxies. Note that the G2 and G3 simulated galaxies lie significantly below the star-forming main sequence defined by the xCOLDGASS sample. (Upper Right) $f_{\rm mol}$ versus $M_\star$ for the same galaxies. The molecular gas fractions of G2 and G3 are significantly lower than those of the PHANGS spiral galaxies. (Lower left) total gas versus $M_\star$. (Lower right) total gas fraction versus $M_\star$. This suggests the (H_2+H I) content in simulated galaxies are also smaller than the observed normal spiral galaxies.

shot. As we can see, the simulated merger still have the similar $\Sigma_{\rm mol}$ and σ_v as the isolated galaxies right before the start of the aphelion passage. Then the molecular gas quickly transitions to a more turbulent state with much higher σ_v after the second passage along with dramatic increase in global SFR, as shown in the snapshot at 2.66 Gyr (bottom panel of Fig. 4). As shown in the zeroth moment map, the G2&G3 merger at this time still shows two separate nuclei, which is at the similar stage as our observed merger, the Antennae and NGC 3256. At this time, the σ_v versus $\Sigma_{\rm mol}$ contours for the simulated mergers lie above the trend seen for the PHANGS galaxies, similar to NGC 3256. In contrast, it is different from the Antennae, which still lies along the trend of PHANGS galaxies. The larger deviation from the PHANGS trend means higher $\alpha_{\rm vir}$. We note that different $\alpha_{\rm CO}$ choices will affect the position of the contour. If we choose ULIRG $\alpha_{\rm CO}$ instead of the Milky Way value, the Antennae would have $\alpha_{\rm vir}$ similar to that of NGC 3256 and our G2&G3 merger. The uncertainty in the correct $\alpha_{\rm CO}$ value to use makes it difficult to interpret the data for the Antennae in this context. For our further analysis, we will adopt the Milky Way $\alpha_{\rm CO}$ for the Antennae (see further discussion in 5.3).

At the post-merger stage after the final coalesce of two nuclei, both $\Sigma_{\rm mol}$ and σ_v reaches its highest value. Fig.

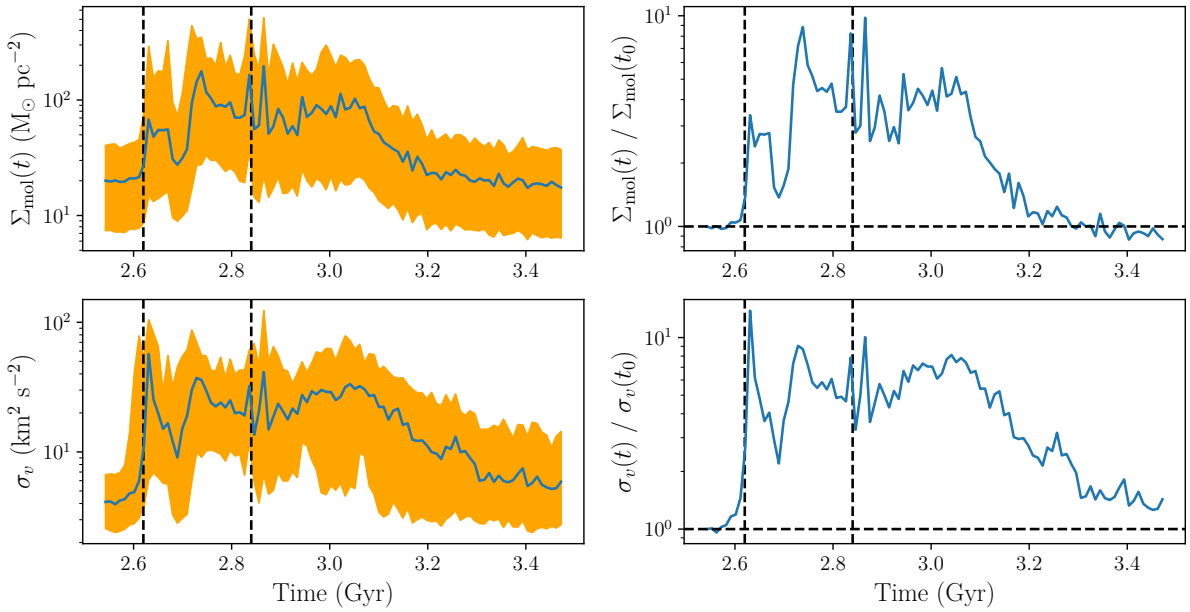

Figure 3. The $\Sigma_{\rm mol}$ and σ_v variation across the second passage and final coalesce of the G2&G3 merger at 'e2' orbit with viewing angle of 'v0'. (Upper left) The $\Sigma_{\rm mol}$ vs time. Blue lines shows the mass weighted median $\Sigma_{\rm mol}$ of the entire merger at that time while the orange filled area indicates $\Sigma_{\rm mol}$ range between 16th and 84th percentile. The two dashed lines indicate the time for the start of the second passage and the final coalesce of two nuclei. (Upper right) The ratio between median $\Sigma_{\rm mol}$ at given time and the median value at the time right before the second passage (t_0 = 2.54 Gyr). (Lower left) the mass weighted median σ_v versus time. (Lower right) the ratio between the median σ_v and σ_v value at t_0.

5 shows the snapshot at 2.87 Gyr when both $\Sigma_{\rm mol}$ and σ_v reaches the maximum. The top and bottom panel shows the measurements from the two viewing angles 'v0' and 'v1' which are roughly perpendicular to each other. We can see that the σ_v versus $\Sigma_{\rm mol}$ contours at this time is generally independent of the viewing angles since most gas is concentrated in the central sphere with roughly 1 kpc diameter. The maximal $\Sigma_{\rm mol}$ at this time reaches 1000 $M_\odot$ pc^{-2}, which is still smaller than the $\Sigma_{\rm mol}$ of the observed mergers. We suspect the lower $\Sigma_{\rm mol}$ in the merger simulations is related to the low global gas fraction in the initial set-up of the simulation. The maximal σ_v reaches 200 km s^{-1} and brings the contour even higher than the trend of NGC 3256, which indicates the $\alpha_{\rm vir}$ at this time is even higher. We will discuss the cause of this in detail in Section 5.2

4.2. *The Dynamical State of GMCs*

During the second passage, we see that the σ_v vs $\Sigma_{\rm mol}$ distribution for our simulated mergers lies above the trend observed for the PHANGS galaxies. A higher σ_v for a given $\Sigma_{\rm mol}$ means the GMCs in these mergers are more turbulent and less gravitationally bound than in normal spiral galaxies. The virial parameter $\alpha_{\rm vir}$ for GMCs in fixed-scale analyses can be calculated as (Sun et al. 2018)

$$\begin{aligned}\alpha_{\rm vir} &= \frac{9\ln 2}{2\pi G}\frac{\sigma_v^2}{\Sigma_{\rm mol} R} \\ &= 5.77\left(\frac{\sigma_v}{\rm km\ s^{-1}}\right)^2\left(\frac{\Sigma_{\rm mol}}{\rm M_\odot}\right)^{-1}\left(\frac{R}{\rm 40pc}\right)^{-1}\end{aligned} \quad (1)$$

where R is the radius of GMCs. In Sun et al. (2018), R is set to be the radius of the beam in the image, as each beam is treated as an independent GMC. For the simulation data, we do not have a telecope beam to convolve with, so we set R to be half the size of each pixel as each pixel can be treated as an independent GMC. With R a constant, $\alpha_{\rm vir}$ depends only on σ_v and $\Sigma_{\rm mol}$. The higher σ_v at a similar $\Sigma_{\rm mol}$ thus implies that $\alpha_{\rm vir}$ values for GMCs in simulated mergers are higher than the values for PHANGS or simulated isolated galaxies. Higher values for $\alpha_{\rm vir}$ are also found for NGC 3256 (Brunetti et al. 2020) and the Antennae (Brunetti 2022; Brunetti, N. et al. in prep). Fig. 6 shows $\alpha_{\rm vir}$ as a function of time during the period near the second pericentric passage for the merger simulation with "e2" orbit and "v0" viewing angle. Initially, $\alpha_{\rm vir}$ is close to the median value in the PHANGS sample. After the collision, $\alpha_{\rm vir}$ increases dramatically, with a median value of ~ 30, which is even higher than in the observed mergers. We note that both Antennae and NGC 3256 are at the very start of second passage (Privon et al. 2013; Renaud et al. 2019a).

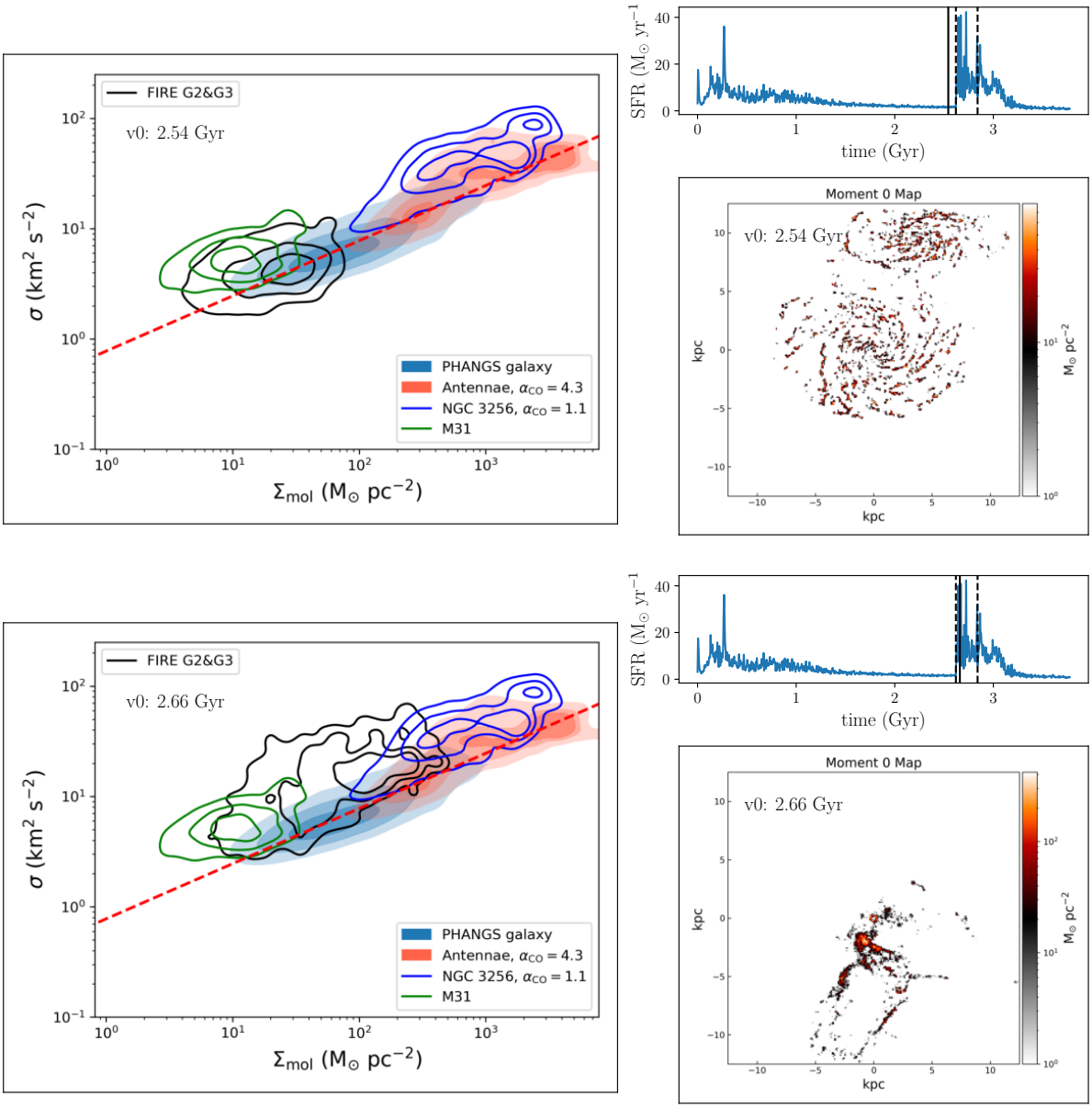

Figure 4. Two of the snapshots for G2&G3 merger with 'e2' orbit with viewing angle of 'v0'. (Top) the snapshot right before the second passage at times of 2.54 Gyr. The left panel shows the σ_v versus $\Sigma_{\rm mol}$ mass weighted contour with the same setting as Fig.1. We also show the density contours for the PHANGS galaxies (filled blue region), NGC 3256 (blue contours) and the Antennae (orange shaded region). For NGC 3256, $\Sigma_{\rm mol}$ is calculated using the ULIRG $\alpha_{\rm CO}$ of 1.1 $M_\odot$ (K km s^{-1} pc^2)$^{-1}$. For the Antennae, gas surface densities is calculated using the Milky Way $\alpha_{\rm CO}$ of 4.3 $M_\odot$ (K km s^{-1} pc^2)$^{-1}$. See Section 5.3 for the detailed discussion on $\alpha_{\rm CO}$ choices. The top right panel shows the SFR history for this merging suite. The black vertical line indicates the time for each snapshot. The two dashed lines indicate the times at the start of second merging and the final coalesce of two nuclei. The lower right panel shows the moment 0 map of the simulated mergers for each snapshot. (Bottom) the snapshot between the second passage and final coalesce at 2.66 Gyr. We can still see two separate nuclei of the simulated merger. The interactive version of the animation are available at https://htmlpreview.github.io/?https://github.com/heh15/merger_animations/blob/main/G2G3_e2_v0.html.

At this stage, we can see $\alpha_{\rm vir}$ still varies dramatically. Therefore, it is possible that the two observed mergers happen to catch the stage of low $\alpha_{\rm vir}$, such as the snapshot shown in the bottom panel of Fig. 4. On the other hand, both simulated and observed mergers have consistently higher $\alpha_{\rm vir}$ than the corresponding isolated galaxies. We will discuss further indication of high $\alpha_{\rm vir}$ in Section 5.2.

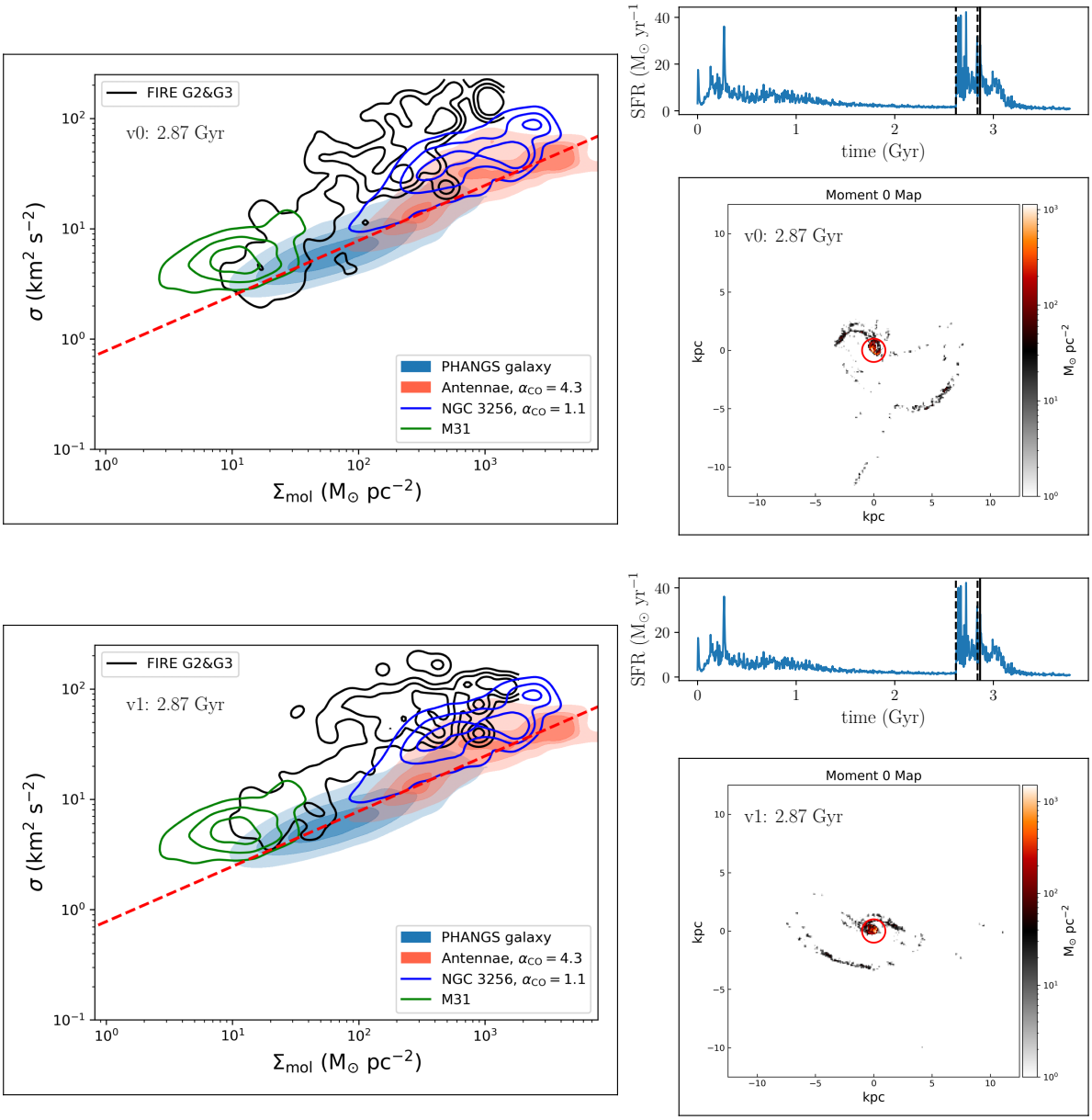

Figure 5. Two of the snapshots for the FIRE-2 merger at time of 2.87 Gyr with viewing angle of 'v0' (upper) and 'v1' (lower). The two line of sights are roughly perpendicular to each other (with angle of 109 degree). The red circle in the moment 0 maps specify the central region within radius of 1 kpc. At this time, the two nuclei has been merged into one with Σ_{mol} reach its highest value. We can see that lots of molecular gas is concentrated in the central 1 kpc spherical region.

We also note that the α_{vir} takes a long time settle back to the original value while SFR value has already returned to normal. The timescale of delay is about 500 Myr, which is much larger than the dynamical timescale of individual GMCs. We suspect this timescale is more related to the dynamical timescale of post-merger itself (e.g. the orbital time).

5. DISCUSSION

5.1. *Gas concentration for simulated mergers*

From moment 0 maps in Fig. 5, we can see that most molecular gas is concentrated in the center during the post merger phase. This is consistent with the traditional scenario that the central starburst activities are caused by the inflow of molecular gas due to the loss of angular momentum (Mihos 1996). To quantify how much fraction of the molecular gas is concentrated in the center, we measure the molecular gas mass in the central 1 kpc circle and calculate the ratio between this value and total molecular gas mass, as shown in Fig. 7. As

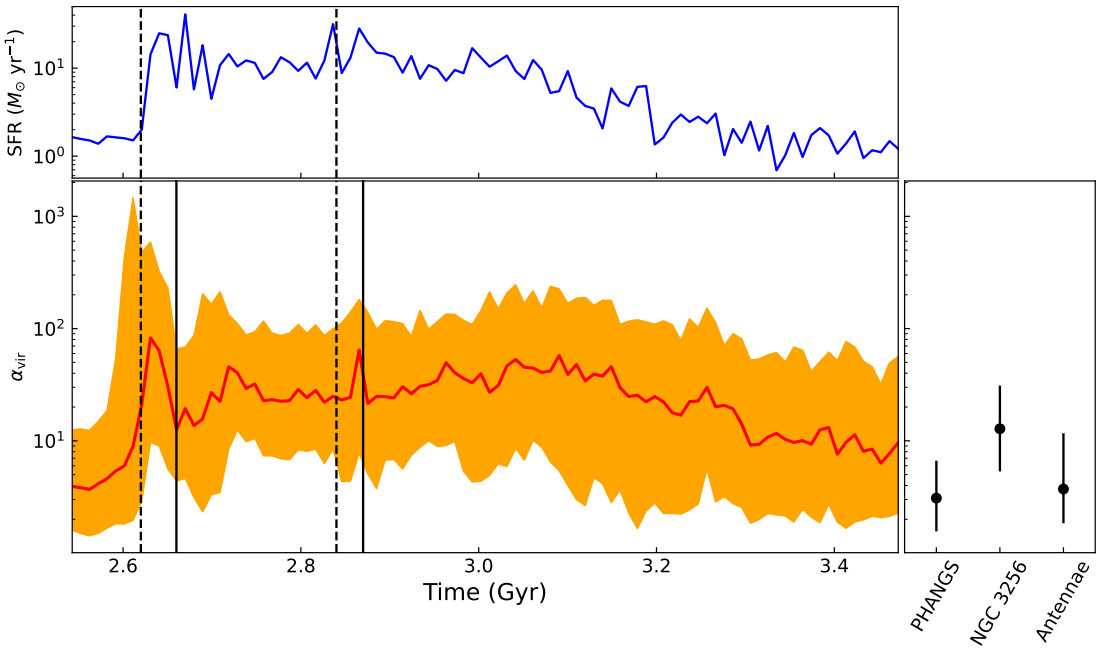

Figure 6. The variation of α_{vir} versus time for the G2&G3 mergers (e2 orbit, v0 viewing angle) during the final coalescence. The red line is the mass weighted median for α_{vir} from the simulation. The orange shaded region includes data within the 16th and 84th quantile of α_{vir} values. The dashed lines correspond to the start of the second passage and the final coalesce of the two nuclei. The two solid lines correspond to the merger times shown in Fig. 4 and 5. The upper panel shows SFR vs time for the second coalescence and the right panel shows the 16th, 50th and 84th quantile of α_{vir} for PHANGS, NGC 3256 and the Antennae from the observations. In calculating α_{vir}, we use the U/LIRG α_{CO} for NGC 3256 and the Milky Way value for PHANGS and the Antennae.

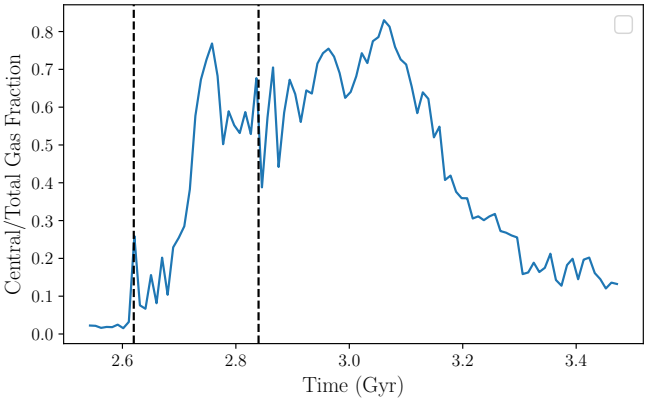

Figure 7. The ratio between molecular gas mass within central 1 kpc radius circle of G3 galaxy and total molecular gas during the second coalesce. We can see that between 2.7 Gyr and 3.1 Gyr more than 60% of molecular gas is concentrated within central 1 kpc region.

we can see, the fraction of molecular gas concentrated in the center reach as high as 80% for a significant period of time ($\sim$ 500 Myr) around the final coalesce. On the other hand, Moreno et al. (2019) shows that the total molecular gas mass is actually decreasing during the second passage. Therefore, the high Σ_{mol} in our simulated mergers compared to isolated galaxies is mostly due to the gas concentration in the center.

5.2. *High σ_v and α_{vir} in simulated mergers*

As shown in Section 4.2, α_{vir} generally stays above 10 during the final coalescence for the G2&G3 merger; these high values are primarily caused by the high velocity dispersion of the gas in the simulation. We also see a similar behavior of high σ_v and α_{vir} for the same merger viewed at a different angle ('v1'). Both α_{vir} and σ_v reach the maximal value right after the final coalesce. From Fig. 5, we can see the high α_{vir} pixels also have high Σ_{mol}, which corresponds to molecular gas in the central 1 kpc region. In the left panel of Fig. 8, we compare the σ_v versus Σ_{mol} distribution for pixels in the central kpc region of G2&G3 merger (red aperture in Fig. 5) at 2.87 Gyr (same as Fig. 5), along with pixels in the center of PHANGS galaxies, the Antennae and NGC 3256. We can see the pixels in the center of G2&G3 merger still have larger deviation from the PHANGS trend than NGC 3256, which indicates it has GMCs with larger α_{vir} in the center. The discrepancy could be caused different gas fractions (Fensch & Bournaud 2021). We also note that the two observed mergers we have are both in quite an early stage after the second passage and for which we can still identify

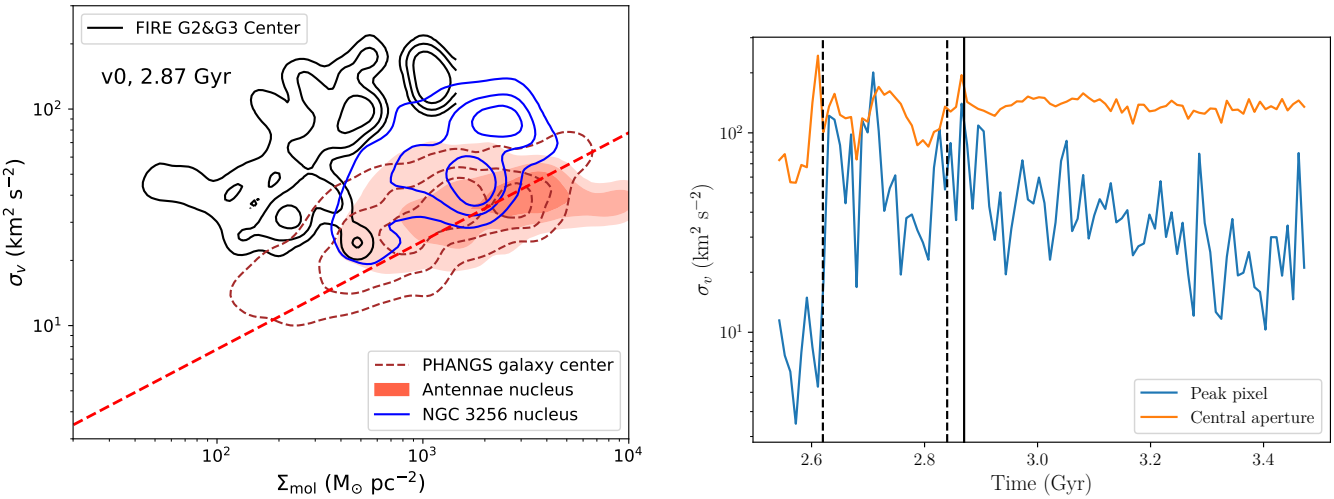

Figure 8. (Left) The σ_v versus $\Sigma_{\rm mol}$ contour for the central 1 kpc region of G2&G3 merger at 2.87 Gyr viewed from 'v0' angle. We also show the contour for the center of PHANGS galaxies (brown dashed contours), Antennae (orange shaded contours) and NGC 3256 (blue contours). (Right) the comparison of σ_v measured for the pixel with peak intensities in the central region (blue line) and σ_v measured for the entire central 1 kpc aperture. The vertical solid line shows the time of snapshot in the left panel. If the two σ_v are equal, it means we are measuring σ_v among multiple clouds instead of intrinsic σ_v of individual GMCs.

two separate nuclei. At this stage, $\alpha_{\rm vir}$ is quite time-sensitive and it is hard to match the exact same stage between the simulated and observed galaxies. Therefore, it is possible that both NGC 3256 and Antennae are caught at a specific merger stage with a lower $\alpha_{\rm vir}$ (although in the case of NGC 3256, still enhanced relative to PHANGS galaxies). In comparison, $\alpha_{\rm vir}$ in the simulations is relatively stable in the post merger stage. This stability suggests that a comparison between simulations and observations of post merger galaxies could be a useful next step. In addition, post mergers have rather simple morphology, which simplifies the task of making quantitative comparisons.

we can also see from Fig. 6 that high global SFR for these mergers throughout the second passage with $\alpha_{\rm vir}$ consistently higher than 10. This is counter-intuitive since we expect low $\alpha_{\rm vir}$ GMCs to form stars. One possible explanation is that our fixed-scale analyses measures the σ_v among multiple clouds along the line of sight instead of the σ_v for a single GMC. We take one snapshot in Fig. 5 as an example. As we can see, most gas is concentrated in the central spherical region with 1 kpc diameter, which is much larger than typical cloud scale of 100 pc. In this case, when we measure the velocity dispersion, we are actually measuring σ_v and the dynamical state of the entire central kpc region, rather than for individual GMCs.

One way to quantify this scenario is to compare the σ_v measured in one pixel with the σ_v measured for the entire aperture of central 1 kpc region. For the pixel σ_v measurement, we choose the pixel with highest surface density in the central region. We would expect the σ_v for pixel measurement trace the internal σ_v of individual GMCs while the σ_v for central aperture at kpc scale are dominated by the velocity differences among different GMCs. If the two σ_v are equal to each other, it is more likely that the pixel σ_v is also dominated by velocity differences among GMCs along the same line of sight. The comparison is shown in the right panel of Fig. 8. We can see the two σ_v at the start shows quite large differences, which is what we expect if we have just one layer of GMCs at the galaxy disk. After the second passage, we see the two values become quite close, which suggests multiple GMCs along the line sight. For our chosen snapshot at 2.87 Gyr, we can see the two values are quite close. This is consistent with the scenario we have discussed in the previous paragraph that the pixel σ_v is tracking the dynamical state of entire central region. At later time after the final coalesce, the σ_v of the brightest pixel drops as the molecular gas starts to settle back to disk again.

5.3. *CO-to-H_2 Conversion Factor Adopted in Mergers*

In observations, the CO-to-H_2 conversion factcor $\alpha_{\rm CO}$ is the key to convert the observed CO luminosity to actual molecular gas mass. The exact value of $\alpha_{\rm CO}$ has large uncertainties and varies significantly among different types of galaxies. Downes & Solomon (1998) find that for starburst U/LIRGs, the $\alpha_{\rm CO}$ value is generally 4 times smaller than that in our Milky Way. Papadopoulos et al. (2012) applied large velocity gradient (LVG) radiative transfer modeling to a large sam-

ple of U/LIRGs and find a consistent α_{CO} of 0.6 $\pm$ 0.2 $M_\odot$ (K km s^{-1} $pc^2)^{-1}$ (excluding the helium contribution). Studies on resolved regions at kpc scale of individual U/LIRGs also show that the starburst regions in these galaxies generally have α_{CO} smaller than commonly adopted value (including Helium) of 1.1 $M_\odot$ (K km s^{-1} $pc^2)^{-1}$ (Sliwa et al. 2012, 2013, 2014, 2017a,b). On the other hand, simulations of mergers also show that α_{CO} will dramatically decrease during the perihelion and aphelion passage between the two galaxies when SFR peaks (Narayanan et al. 2011; Renaud et al. 2019a). These studies clearly show that starburst activity can significantly reduce the value of α_{CO}.

Sargent et al. (2014) propose a prescription for determining α_{CO} for an individual galaxy as

$$\alpha_{CO} = (1 - f_{SB}) \times \alpha_{CO,MS} + f_{SB} \times \alpha_{CO,SB} \quad (2)$$

where $\alpha_{CO,MS}$ and $\alpha_{CO,SB}$ are the conversion factors for the Milky Way (4.3 $M_\odot$ (K km s^{-1} $pc^2)^{-1}$) and U/LIRGs (1.1 $M_\odot$ (K km s^{-1} $pc^2)^{-1}$, including helium), and f_{SB} is the probability for a galaxy to be a starburst galaxy, which is determined by its deviation from the star forming main sequence. We adopt the star forming main sequence relation from Catinella et al. (2018),

$$\log \mathrm{sSFR}_{MS} = -0.344(\log M_\star - 9) - 9.822 \quad (3)$$

where sSFR = SFR / $M_\star$ is the specific star formation rate.We can then calculate the ratio of actual measured sSFR divided the sSFR_{MS} at main sequence for a given $M_\star$ to determine f_{SB}. NGC 3256 has an $\mathrm{sSFR/sSFR}_{MS}$ ratio of 15 (Brunetti et al. 2020), which suggests NGC 3256 should have α_{CO} close to the U/LIRG value.

However, the Antennae has a SFR of 8.5 $M_\odot yr^{-1}$ and $M_\star$ of 4.5 $\times$ 10^{10} $M_\odot$, which gives us an $\mathrm{sSFR/sSFR}_{MS}$ ratio of 4.85, which also suggests that α_{CO} in the Antennae should be quite close to the U/LIRG value. However, various evidence suggests that α_{CO} in the Antennae might be closer to the Milky-Way value of 4.3 $M_\odot$ (K km s^{-1} $pc^2)^{-1}$. Wilson et al. (2003) estimate α_{CO} to be about 6.5 $M_\odot$ (K km s^{-1} $pc^2)^{-1}$ for super giant molecular complexes (SGMCs) in the Antennae overlap region based on virial mass estimates. Schirm et al. (2014) find the global α_{CO} of the Antennae to be 7 $M_\odot$ (K km s^{-1} $pc^2)^{-1}$ based on large velocity gradient (LVG) radiative transfer modeling of Herschel CO and C I lines on kpc scales. In simulations, Renaud et al. (2019a) have modeled Antennae-like galaxies and their best match to the current observed stage for the Antennae suggests an α_{CO} of 2.8 $M_\odot$ (K km s^{-1} $pc^2)^{-1}$. Based on this previous work, we have adopted the Milky Way α_{CO} for the Antennae.

5.4. *Comparison with other simulations*

In this work, we use the non-cosmological simulations from Moreno et al. (2019) to compare GMC properties in mergers and normal spiral galaxies. Two major advantages of this simulation suite are that it has a resolution of 1.1 pc (which is much smaller than typical GMC scales) and it can model the ISM down to low temperatures ($\sim$ 10 K), both of which allow us to match the molecular gas in simulations with the CO observations. Various cosmological simulations show that mergers are responsible for enhancing molecular gas fraction and triggering starburst activities (Scudder et al. 2015; Knapen et al. 2015; Patton et al. 2013; Martin et al. 2017; Rodríguez Montero et al. 2019; Patton et al. 2020, e.g.,). However, these simulations can only model gas with temperature down to 10^4 K and hence are more focused on the global gas properties of mergers. An alternative choice is to compare observations with cosmological zoom-in simulations, which allows for higher resolution, more realistic feedback star formation thresholds and more realistic modeling of the multi-phase ISM. Various authors have explored GMC properties, mostly in Milky-Way like galaxies (e.g. Guedes et al. 2011; Ceverino et al. 2014; Sawala et al. 2014; Benincasa et al. 2020), and they generally reproduce the GMC mass function in our Milky Way. However, little work has been done for GMCs in mergers. In addition, the Milky Way is identified as a green-valley galaxy (Mutch et al. 2011) with lower SFR than typical spiral galaxies in the local universe. Therefore, due to the lack of zoom-in cosmological simulations on local mergers, we adopt the idealized simulations for this study. Furthermore, idealized simulations allow us to compare GMCs of control galaxies with those of mergers to directly study the impact of the merging event.

Several idealized simulations have been performed to study molecular gas and GMC properties in mergers and we mention a few of the most relevant works here. Li et al. (2022) perform a study of GMCs and young massive star clusters (YMCs) in Antennae-like mergers. They find that GMC mass functions for mergers have similar power-law slopes to normal spirals during the second coalescence but with much higher mass values. Narayanan et al. (2011) compare the α_{CO} in mergers and normal spiral galaxies and find that low α_{CO} in mergers is mostly due to the high temperature and α_{vir} of GMCs in the merger. They predict there is a transition stage with α_{CO} between U/LIRG and Milky Way values. In contrast, Renaud et al. (2019b) show that α_{CO} values drop quickly during each coalescence between two galaxies. We find similar behavior for α_{vir} during the second coalesce, which is what we expect if α_{vir} is tightly anti-

correlated with α_{CO} as suggested in Narayanan et al. (2011).

6. CONCLUSIONS

We summarize our main conclusions below:

- Our pixel-by-pixel analysis shows that GMCs in the simulated isolated FIRE-2 galaxies (G2 and G3) lie along the same trend as GMCs in the PHANGS galaxies. However, the Σ_{mol} values of the isolated FIRE-2 galaxies are significantly lower than those of the PHANGS galaxies. Instead, the simulated Σ_{mol} values lie closer to M 31, which is identified as a green-valley galaxy with a low star formation rate for its stellar mass. The low gas surface density cannot be corrected for by viewing the simulations at different inclination angles.

- The global molecular gas mass fractions of the simulated galaxies are lower than those of the PHANGS galaxies. The total (HI+H_2) gas fractions for the simulated galaxies are also lower than the observations. In global gas fraction, the simulated galaxies are more similar to green valley galaxies like the Milky Way or M31 than to the normal spiral galaxies in PHANGS. These low global gas fractions likely play a role in limiting the maximum values of Σ_{mol} seen in the mergers.

- We plot σ_v vs Σ_{mol} for our simulated galaxy mergers. GMCs in the mergers have significantly higher σ_v, and thus lie above the PHANGS σ_v $-\Sigma_{mol}$ trend. However, Σ_{mol} values in the simulated mergers are still lower than those of the two observed mergers, NGC 3256 and the Antennae. These low Σ_{mol} values may be caused by initial set-up of progenitor galaxies in the simulations that results in low global cold gas fractions (see previous point).

- We calculate the virial parameter, α_{vir}, for GMCs in the simulated mergers. α_{vir} values in the simulations are higher than in the observed mergers during the period of the second passage. This discrepancy may be related to the very small sample (two!) of observed mergers with GMC-scale data for their molecular gas.

In the future, we would like to expand our comparison on more observed and simulated mergers. From the observational side, we need larger samples of galaxy mergers spanning different evolutionary stages in order to understand how GMCs evolve throughout the merging. In addition, it is easier to compare the observation with simulation at postmerger stage since the morphology is simpler and easier to quantify. In the ALMA archive, we have already had at least 10 U/LIRGs with GMC resolution CO 2-1 observations. We can utilize these archival data to build a more complete sample of GMCs in mergers at different stages. From the simulation side, we can see that the initial set-up could affect our interpretation on the simulation results. Therefore, it is necessary for us to compare with simulations that better match the observed galaxies. For the two observed mergers we have, Antennae has been widely studied and matched by non-cosmological simulations (e.g. Renaud et al. 2019a; Li et al. 2022). Besides comparing with these non-cosmological simulations, we could also compare observation with some latest cosmological simulations, such as FIREBox (Feldmann et al. 2021), that includes local mergers.

Facilities: HST(STIS), Swift(XRT and UVOT), AAVSO, CTIO:1.3m, CTIO:1.5m,CXO

REFERENCES

Benincasa, S. M., Loebman, S. R., Wetzel, A., et al. 2020, Monthly Notices of the Royal Astronomical Society, 497, 3993, doi: 10.1093/mnras/staa2116

Bottrell, C., & Hani, M. H. 2022, Monthly Notices of the Royal Astronomical Society, 514, 2821, doi: 10.1093/mnras/stac1532

Bottrell, C., Hani, M. H., Teimoorinia, H., Patton, D. R., & Ellison, S. L. 2022, Monthly Notices of the Royal Astronomical Society, 511, 100, doi: 10.1093/mnras/stab3717

Bottrell, C., Hani, M. H., Teimoorinia, H., et al. 2019, Monthly Notices of the Royal Astronomical Society, 490, 5390, doi: 10.1093/mnras/stz2934

Bournaud, F., Duc, P. A., & Emsellem, E. 2008, Monthly Notices of the Royal Astronomical Society, 389, L8, doi: 10.1111/j.1745-3933.2008.00511.x

Brunetti, N. 2022, Thesis. https://macsphere.mcmaster.ca/handle/11375/27447

Brunetti, N., & Wilson, C. D. 2022, Monthly Notices of the Royal Astronomical Society, 515, 2928, doi: 10.1093/mnras/stac1975

Brunetti, N., Wilson, C. D., Sliwa, K., et al. 2020, Monthly Notices of the Royal Astronomical Society, 500, 4730, doi: 10.1093/mnras/staa3425

Catinella, B., Saintonge, A., Janowiecki, S., et al. 2018, Monthly Notices of the Royal Astronomical Society, 476, 875, doi: 10.1093/mnras/sty089

Ceverino, D., Klypin, A., Klimek, E. S., et al. 2014, Monthly Notices of the Royal Astronomical Society, 442, 1545, doi: 10.1093/mnras/stu956

Colombo, D., Hughes, A., Schinnerer, E., et al. 2014, The Astrophysical Journal, 784, 3, doi: 10.1088/0004-637X/784/1/3

Colombo, D., Rosolowsky, E., Duarte-Cabral, A., et al. 2019, Monthly Notices of the Royal Astronomical Society, 483, 4291, doi: 10.1093/mnras/sty3283

Dale, J. E., Ngoumou, J., Ercolano, B., & Bonnell, I. A. 2014, Monthly Notices of the Royal Astronomical Society, 442, 694, doi: 10.1093/mnras/stu816

Decataldo, D., Lupi, A., Ferrara, A., Pallottini, A., & Fumagalli, M. 2020, Monthly Notices of the Royal Astronomical Society, 497, 4718, doi: 10.1093/mnras/staa2326

Donovan Meyer, J., Koda, J., Momose, R., et al. 2013, The Astrophysical Journal, 772, 107, doi: 10.1088/0004-637X/772/2/107

Downes, D., & Solomon, P. M. 1998, ApJ, 507, 615, doi: 10.1086/306339

Fall, S. M., Krumholz, M. R., & Matzner, C. D. 2010, Astrophysical Journal Letters, 710, 142, doi: 10.1088/2041-8205/710/2/L142

Feldmann, R., & Gnedin, N. Y. 2011, The Astrophysical Journal, 727, L12, doi: 10.1088/2041-8205/727/1/L12

Fensch, J., & Bournaud, F. 2021, Monthly Notices of the Royal Astronomical Society, 505, 3579, doi: 10.1093/mnras/stab1489

Fensch, J., Renaud, F., Bournaud, F., et al. 2017, Monthly Notices of the Royal Astronomical Society, 465, 1934, doi: 10.1093/mnras/stw2920

Fukui, Y., Kawamura, A., Minamidani, T., et al. 2008, The Astrophysical Journal Supplement Series, 178, 56, doi: 10.1086/589833

Grudić, M. Y., Hopkins, P. F., Faucher-Giguère, C. A., et al. 2018, Monthly Notices of the Royal Astronomical Society, 475, 3511, doi: 10.1093/MNRAS/STY035

Guedes, J., Callegari, S., Madau, P., & Mayer, L. 2011, The Astrophysical Journal, 742, 76, doi: 10.1088/0004-637X/742/2/76

Guszejnov, D., Hopkins, P. F., & Ma, X. 2017, Monthly Notices of the Royal Astronomical Society, 472, 2107, doi: 10.1093/mnras/stx2067

Heyer, M., & Dame, T. M. 2015, Annual Review of Astronomy and Astrophysics, vol. 53, p.583-629, 53, 583, doi: 10.1146/annurev-astro-082214-122324

Heyer, M., Krawczyk, C., Duval, J., & Jackson, J. M. 2009, The Astrophysical Journal, 699, 1092, doi: 10.1088/0004-637X/699/2/1092

Hopkins, P. F. 2015, Monthly Notices of the Royal Astronomical Society, 450, 53, doi: 10.1093/mnras/stv195

—. 2017, A New Public Release of the GIZMO Code, Tech. rep. https://ui.adsabs.harvard.edu/abs/2017arXiv171201294H

Hopkins, P. F., Wetzel, A., Kereš, D., et al. 2018, Monthly Notices of the Royal Astronomical Society, 480, 800, doi: 10.1093/mnras/sty1690

Howard, C. S., Pudritz, R. E., & Harris, W. E. 2018, Nature Astronomy, 2, 725, doi: 10.1038/s41550-018-0506-0

Hughes, A., Meidt, S. E., Colombo, D., et al. 2013, The Astrophysical Journal, 779, 46, doi: 10.1088/0004-637X/779/1/46

Jeffreson, S. M. R., & Kruijssen, J. M. D. 2018, Monthly Notices of the Royal Astronomical Society, 28, 1, doi: 10.1093/mnras/sty594

Kennicutt, R. C., & Evans, N. J. 2012, Annual Review of Astronomy and Astrophysics, 50, 531, doi: 10.1146/annurev-astro-081811-125610

Kennicutt, Jr., R. C. 1998, The Astrophysical Journal, 498, 541, doi: 10.1086/305588

Kim, C.-G., Ostriker, E. C., & Raileanu, R. 2017, The Astrophysical Journal, 834, 25, doi: 10.3847/1538-4357/834/1/25

Knapen, J. H., Cisternas, M., & Querejeta, M. 2015, Monthly Notices of the Royal Astronomical Society, 454, 1742, doi: 10.1093/mnras/stv2135

Kruijssen, J. M., Longmore, S. N., Elmegreen, B. G., et al. 2014, Monthly Notices of the Royal Astronomical Society, 440, 3370, doi: 10.1093/mnras/stu494

Kruijssen, J. M. D., Schruba, A., Hygate, A. P. S., et al. 2018, Monthly Notices of the Royal Astronomical Society, 479, 1866, doi: 10.1093/mnras/sty1128

Lada, C. J., & Dame, T. M. 2020, The Astrophysical Journal, 898, 3, doi: 10.3847/1538-4357/ab9bfb

Larson, R. B. 1981, Monthly Notices of the Royal Astronomical Society, 194, 809, doi: 10.1093/mnras/194.4.809

Lee, E. J., Miville-Deschênes, M.-A., & Murray, N. W. 2016, The Astrophysical Journal, 833, 229, doi: 10.3847/1538-4357/833/2/229

Leitherer, C., Schaerer, D., Goldader, J. D., et al. 1999, The Astrophysical Journal Supplement Series, 123, 3, doi: 10.1086/313233

Leroy, A. K., Hughes, A., Schruba, A., et al. 2016, The Astrophysical Journal, 831, 16, doi: 10.3847/0004-637X/831/1/16

Leroy, A. K., Schinnerer, E., Hughes, A., et al. 2021, ApJS, 257, 43, doi: 10.3847/1538-4365/ac17f3

Li, H., Vogelsberger, M., Bryan, G. L., et al. 2022, Monthly Notices of the Royal Astronomical Society, 514, 265, doi: 10.1093/mnras/stac1136

Li, H., Vogelsberger, M., Marinacci, F., & Gnedin, O. Y. 2019, Monthly Notices of the Royal Astronomical Society, 487, 364, doi: 10.1093/mnras/stz1271

Martin, G., Kaviraj, S., Devriendt, J. E. G., et al. 2017, Monthly Notices of the Royal Astronomical Society, 472, L50, doi: 10.1093/mnrasl/slx136

McElroy, R., Bottrell, C., Hani, M. H., et al. 2022, Monthly Notices of the Royal Astronomical Society, 515, 3406, doi: 10.1093/mnras/stac1715

McMullin, J. P., Waters, B., Schiebel, D., Young, W., & Golap, K. 2007, 376, 127. https://ui.adsabs.harvard.edu/abs/2007ASPC..376..127M

Mihos, J. C. 1996

Miville-Deschênes, M.-A., Murray, N., & Lee, E. J. 2017, The Astrophysical Journal, 834, 57, doi: 10.3847/1538-4357/834/1/57

Moreno, J., Torrey, P., Ellison, S. L., et al. 2019, Monthly Notices of the Royal Astronomical Society, 485, 1320, doi: 10.1093/mnras/stz417

—. 2021, Monthly Notices of the Royal Astronomical Society, 503, 3113, doi: 10.1093/mnras/staa2952

Muraoka, K., Kohno, K., Tosaki, T., et al. 2009, The Astrophysical Journal, 706, 1213, doi: 10.1088/0004-637X/706/2/1213

Murray, N., Quataert, E., & Thompson, T. A. 2010, The Astrophysical Journal, 709, 191, doi: 10.1088/0004-637X/709/1/191

Mutch, S. J., Croton, D. J., & Poole, G. B. 2011, The Astrophysical Journal, 736, 84, doi: 10.1088/0004-637X/736/2/84

Myers, A. T., Klein, R. I., Krumholz, M. R., & McKee, C. F. 2014, Monthly Notices of the Royal Astronomical Society, 439, 3420, doi: 10.1093/mnras/stu190

Narayanan, D., Krumholz, M., Ostriker, E. C., & Hernquist, L. 2011, Monthly Notices of the Royal Astronomical Society, 418, 664, doi: 10.1111/j.1365-2966.2011.19516.x

Nieten, C., Neininger, N., Guélin, M., et al. 2006, Astronomy and Astrophysics, Volume 453, Issue 2, July II 2006, pp.459-475, 453, 459, doi: 10.1051/0004-6361:20035672

Orr, M. E., Hayward, C. C., Hopkins, P. F., et al. 2018, Monthly Notices of the Royal Astronomical Society, 478, 3653, doi: 10.1093/mnras/sty1241

Papadopoulos, P. P., van der Werf, P. P., Xilouris, E. M., et al. 2012, Monthly Notices of the Royal Astronomical Society, 426, 2601, doi: 10.1111/j.1365-2966.2012.21001.x

Patton, D. R., Torrey, P., Ellison, S. L., Mendel, J. T., & Scudder, J. M. 2013, Monthly Notices of the Royal Astronomical Society, 433, L59, doi: 10.1093/mnrasl/slt058

Patton, D. R., Wilson, K. D., Metrow, C. J., et al. 2020, Monthly Notices of the Royal Astronomical Society, 494, 4969, doi: 10.1093/mnras/staa913

Privon, G. C., Barnes, J. E., Evans, A. S., et al. 2013, Astrophysical Journal, 771, doi: 10.1088/0004-637X/771/2/120

Raskutti, S., Ostriker, E. C., & Skinner, M. A. 2016, The Astrophysical Journal, 829, 130, doi: 10.3847/0004-637X/829/2/130

Renaud, F., Bournaud, F., Agertz, O., et al. 2019a, Astronomy & Astrophysics, 625, A65, doi: 10.1051/0004-6361/201935222

Renaud, F., Bournaud, F., Daddi, E., & Weiß, A. 2019b, Astronomy & Astrophysics, Volume 621, id.A104, <NUMPAGES>5</NUMPAGES> pp., 621, A104, doi: 10.1051/0004-6361/201834397

Renaud, F., Bournaud, F., Kraljic, K., & Duc, P. A. 2014, Monthly Notices of the Royal Astronomical Society: Letters, 442, doi: 10.1093/mnrasl/slu050

Rice, T. S., Goodman, A. A., Bergin, E. A., Beaumont, C., & Dame, T. M. 2016, The Astrophysical Journal, 822, 52, doi: 10.3847/0004-637X/822/1/52

Rico-Villas, F., Martin-Pintado, J., Gonzalez-Alfonso, E., Martin, S., & Rivilla, V. M. 2020, Monthly Notices of the Royal Astronomical Society, 491, 4573, doi: 10.1093/mnras/stz3347

Robertson, B., Bullock, J. S., Cox, T. J., et al. 2006, The Astrophysical Journal, 645, 986, doi: 10.1086/504412

Rodríguez Montero, F., Davé, R., Wild, V., Anglés-Alcázar, D., & Narayanan, D. 2019, Monthly Notices of the Royal Astronomical Society, 490, 2139, doi: 10.1093/mnras/stz2580

Roman-Duval, J., Jackson, J. M., Heyer, M., Rathborne, J., & Simon, R. 2010, The Astrophysical Journal, 723, 492, doi: 10.1088/0004-637X/723/1/492

Saintonge, A., Catinella, B., Tacconi, L. J., et al. 2017, The Astrophysical Journal Supplement Series, 233, 22, doi: 10.3847/1538-4365/aa97e0

Sakamoto, K., Aalto, S., Combes, F., Evans, A., & Peck, A. 2014, The Astrophysical Journal, 797, 90, doi: 10.1088/0004-637X/797/2/90

Sargent, M. T., Daddi, E., Béthermin, M., et al. 2014, Astrophysical Journal, 793, doi: 10.1088/0004-637X/793/1/19

Sawala, T., Frenk, C. S., Fattahi, A., et al. 2014, Local Group galaxies emerge from the dark, Tech. rep. https://ui.adsabs.harvard.edu/abs/2014arXiv1412.2748S

Schirm, M. R. P., Wilson, C. D., Parkin, T. J., et al. 2014, The Astrophysical Journal, 781, 101, doi: 10.1088/0004-637X/781/2/101

Schruba, A., Kruijssen, J. M. D., & Leroy, A. K. 2019, The Astrophysical Journal, 883, 2, doi: 10.3847/1538-4357/ab3a43

Scudder, J. M., Ellison, S. L., Momjian, E., et al. 2015, Monthly Notices of the Royal Astronomical Society, 449, 3719, doi: 10.1093/mnras/stv588

Seillé, L. M., Buat, V., Haddad, W., et al. 2022, Spatial disconnection between stellar and dust emissions: the test of the Antennae Galaxies (Arp 244), Tech. rep. https://ui.adsabs.harvard.edu/abs/2022arXiv220707967S

Sick, J., Courteau, S., Cuillandre, J.-C., et al. 2015, 311, 82, doi: 10.1017/S1743921315003440

Sliwa, K., Wilson, C. D., Aalto, S., & Privon, G. C. 2017a, The Astrophysical Journal, 840, L11, doi: 10.3847/2041-8213/aa6ea4

Sliwa, K., Wilson, C. D., Iono, D., Peck, A., & Matsushita, S. 2014, The Astrophysical Journal, 796, L15, doi: 10.1088/2041-8205/796/1/L15

Sliwa, K., Wilson, C. D., Matsushita, S., et al. 2017b, The Astrophysical Journal, 840, 8, doi: 10.3847/1538-4357/aa689b

Sliwa, K., Wilson, C. D., Petitpas, G. R., et al. 2012, Astrophysical Journal, 753, doi: 10.1088/0004-637X/753/1/46

Sliwa, K., Wilson, C. D., Krips, M., et al. 2013, Astrophysical Journal, 777, doi: 10.1088/0004-637X/777/2/126

Sun, J., Leroy, A. K., Schruba, A., et al. 2018, The Astrophysical Journal, 860, 172, doi: 10.3847/1538-4357/aac326

Sun, J., Leroy, A. K., Schinnerer, E., et al. 2020, ApJL, 901, L8, doi: 10.3847/2041-8213/abb3be

Sun, J., Leroy, A. K., Rosolowsky, E., et al. 2022, The Astronomical Journal, 164, 43, doi: 10.3847/1538-3881/ac74bd

Teyssier, R., Chapon, D., & Bournaud, F. 2010, Astrophysical Journal Letters, 720, 149, doi: 10.1088/2041-8205/720/2/L149

Torrey, P., Hopkins, P. F., Faucher-Giguère, C.-A., et al. 2017, Monthly Notices of the Royal Astronomical Society, 467, 2301, doi: 10.1093/mnras/stx254

Tosaki, T., Kohno, K., Harada, N., et al. 2017, Publications of the Astronomical Society of Japan, 69, 18, doi: 10.1093/pasj/psw122

Wellons, S., Faucher-Giguère, C.-A., Hopkins, P. F., et al. 2022, Exploring supermassive black hole physics and galaxy quenching across halo mass in FIRE cosmological zoom simulations, Tech. rep. https://ui.adsabs.harvard.edu/abs/2022arXiv220306201W

Wilson, C. D., Scoville, N., Madden, S. C., & Charmandaris, V. 2003, The Astrophysical Journal, 599, 1049, doi: 10.1086/379344